11th World Congress on Computational Mechanics (WCCM XI)
5th European Conference on Computational Mechanics (ECCM V)
6th European Conference on Computational Fluid Dynamics (ECFD VI)
E. Oñate, J. Oliver and A. Huerta (Eds)

DISCRETE MODELING OF STRAIN ACCUMULATION IN GRANULAR SOILS UNDER CYCLIC LOADING

Ngoc-Son Nguyen, Stijn François and Geert Degrande

KU Leuven, Department of Civil Engineering, Structural Mechanics
Kasteelpark Arenberg 40, 3001 Leuven, Belgium

Key words: Granular soils, cyclic loading, strain accumulation, discrete element method

Abstract. This paper presents a study of strain accumulation in granular soils under vibration by using the discrete element method. A loose and a medium dense sample composed of a relatively large number of spheres are simulated. A series of stress controlled cyclic triaxial tests with different excitation amplitudes and frequencies is performed on these samples at different static stress states. The study focuses on the influence of different factors on strain accumulation such as the sample density, the cyclic excitation amplitude and frequency and the static stress state. In addition, the evolution of the internal structure of the granular samples is also investigated.

1 INTRODUCTION

Road and railway traffic induced vibrations cause the stress state in soils to vary cyclically with low amplitude compared to the stress state and relatively high frequency. The excitation frequency can be typically around 10 - 15 Hz for road traffic induced vibrations [1] and around 40 - 80 Hz for railway traffic induced vibrations [2]. Under the action of vibrations, granular soils under the foundation of buildings accumulate strain, which might cause differential settlement, hence damage to buildings. A profound understanding of strain accumulation in granular soils is very important to advance the ability to predict this phenomenon.

Strain accumulation in granular soils has been studied in the laboratory by using cyclic tests performed at low frequency [3, 4]. At high frequency (typically higher than 10 Hz), the accuracy of cyclic tests is significantly reduced [5]. The numerical simulation with the discrete element method (DEM) pioneered by Cundall and Strack [6] can complement laboratory experiments. The DEM is suitable to simulate cyclic tests at high frequency. Moreover, this method allows an investigation of the microscopic behavior of granular samples during cyclic excitation as it is possible to access to information at the particle level.

This paper presents a study of strain accumulation in granular soils induced by vibrations by using the DEM. Numerical simulations are performed with the software PFC3D [7]. 3D granular samples composed of a relatively large number of spheres (about 10000) are considered. This study aims at analyzing the influence of different factors such as the sample density, the amplitude and frequency of the cyclic excitation and the static stress state on strain accumulation in granular soils. In addition, the local behavior of granular samples during low amplitude cyclic excitation is investigated.

This paper is organized as follows. Section 2 presents two numerical samples considered in the current study. The behavior of these samples during triaxial compression tests is briefly discussed in section 3. Strain accumulation in these samples during low amplitude cyclic triaxial tests is presented in section 4.

2 NUMERICAL SAMPLES

Two samples A and B with different densities are created, each of which is composed of 10342 spheres with mass density $\rho = 2650$ kg/m^3. The linear contact model [7] with normal stiffness $k_\mathrm{n} = 5 \times 10^6$ N/m, tangential stiffness $k_\mathrm{s} = k_\mathrm{n}$ and friction coefficient $\mu = 0.6$ is adopted in the current study. No viscous damping is added at the contact points; therefore, only friction dissipates energy in the samples.

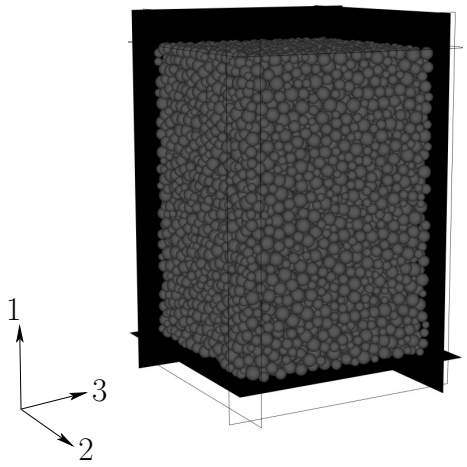

Figure 1: Sample contained by a parallelepiped composed of 6 rigid walls.

The particles of each sample are randomly generated in a parallelepiped composed of 6 rigid walls (figure 1). The samples are then compacted by compression in the three directions until reaching a given target stress state. To obtain different densities, the friction coefficient μ for samples A and B is set to 0.6 and 0.3 during the compaction phase, respectively. When about 90% of the target stress state is reached, μ is reset to its original value. After compaction, the porosity n is 0.43 for sample A and 0.41 for sample

B at a confinement stress $\sigma_{11} = \sigma_{22} = \sigma_{33} = \sigma_o = 50$ kPa and both samples are isotropic.

The stress tensor $\boldsymbol{\sigma}$ and strain tensor $\boldsymbol{\varepsilon}$ of each sample are defined from the contact forces applied by the walls on the sample and the displacement of the walls [8]. The sign convention used in this paper is that tensile stresses and strains are positive. For triaxial loading, the mean stress p and the deviatoric stress q are defined as $p = (\sigma_{11} + 2\sigma_{33})/3$ and $q = \mid \sigma_{11} - \sigma_{33} \mid$. The volumetric strain ε_{v} and the deviatoric strain ε_{d} are defined as $\varepsilon_{\mathrm{v}} = \varepsilon_{11} + 2\varepsilon_{33}$ and $\varepsilon_{\mathrm{d}} = 2 \mid \varepsilon_{11} - \varepsilon_{33} \mid /3$.

3 TRIAXIAL COMPRESSION TESTS

Quasi-static triaxial compression tests are performed on samples A and B by approaching slowly the top and bottom walls and keeping the lateral stresses σ_{22} and σ_{33} equal to the confinement stress σ_o. Figure 2 shows the stress ratio $\eta = q/ \mid p \mid$ and the volumetric strain ε_{v} versus the axial strain ε_{11} for two tests performed on samples A and B at $\sigma_{\mathrm{o}} =$ 50 kPa. The figure shows that sample A presents the behavior of a loose granular sample, while sample B presents the behavior of a medium dense one. These samples first contract and then dilate. The state at which this transition occurs is called the characteristic state. For sample A the characteristic state occurs at large deformation ($\varepsilon_{11} \approx$ -0.074), while for sample B this state occurs at small deformation ($\varepsilon_{11} \approx$ -0.009). Lines $\mathrm{L_A}$ and $\mathrm{L_B}$ drawn in figure 2 depict the characteristic state for samples A and B, respectively.

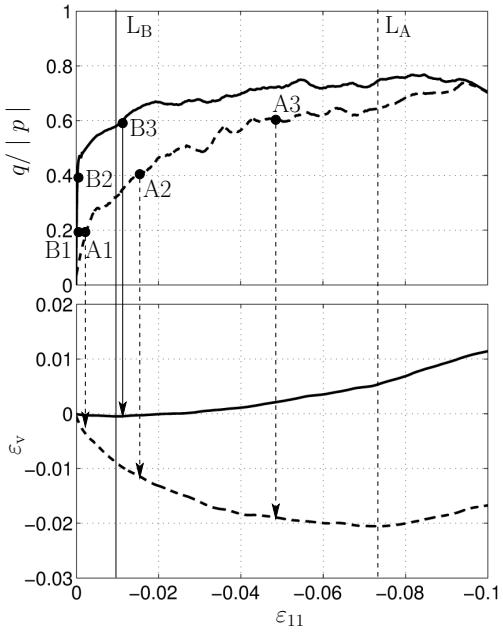

Figure 2: Stress ratio $\eta = q/ \mid p \mid$ and volumetric strain ε_{v} versus axial strain ε_{11} for two triaxial compression tests applied on samples A (dashed line) and B (solid line) at a confinement stress $\sigma_{\mathrm{o}} = 50$ kPa.

Points A1, A2 and A3 drawn on the curve for sample A and points B1, B2 and B3 drawn on the curve for sample B represent the stress states at which cyclic excitations are applied (these loadings are presented in section 4). The arrows indicate the volumetric behavior of each sample at the corresponding stress states. The volumetric behavior of a sample at a given stress state is quantified by the strain increment ratio $\Delta\varepsilon_{\mathrm{v}}/\Delta\varepsilon_{\mathrm{d}}$ computed with a strain increment tensor $\Delta\boldsymbol{\varepsilon}$ starting from this stress state. Table 1 shows the stress ratio η and the strain increment ratio $\Delta\varepsilon_{\mathrm{v}}/\Delta\varepsilon_{\mathrm{d}}$ at these points. Sample A tends to contract less from point A1 to point A3; the same tendency is observed for sample B from point B1 to point B3. In particular, at point B3, sample B slightly dilates.

Sample	Point	η	$\Delta\varepsilon_{\mathrm{v}}/\Delta\varepsilon_{\mathrm{d}}$
A	A1	0.2	-0.70
	A2	0.4	-0.26
	A3	0.6	-0.16
B	B1	0.2	-0.40
	B2	0.4	-0.06
	B3	0.6	0.01

Table 1: Stress ratio η and strain increment ratio $\Delta\varepsilon_{\mathrm{v}}/\Delta\varepsilon_{\mathrm{d}}$ at points A1, A2, A3, B1, B2 and B3 in figure 2.

4 LOW AMPLITUDE CYCLIC TRIAXIAL TESTS

To perform a cyclic triaxial test on a sample, the sample is first consolidated by triaxial compression until the stress state reaches the target average stress state ($\sigma_{11} = \overline{\sigma}_{11}$ and $\sigma_{22} = \sigma_{33} = \sigma_{\mathrm{o}}$ with $\overline{\sigma}_{11}$ the target average axial stress). The axial stress σ_{11} is then cycled between the lower and upper values $\overline{\sigma}_{11} \pm \sigma_{11}^{\mathrm{cyc}}$ with $\sigma_{11}^{\mathrm{cyc}}$ the cyclic stress amplitude and the lateral stresses σ_{22} and σ_{33} are kept equal to the confinement stress σ_{o}. The cyclic stress σ_{11} is applied by moving cyclically the top and bottom walls inward and outward until σ_{11} reaches the upper and lower values, respectively. By doing so, the amplitude $\sigma_{11}^{\mathrm{cyc}}$ can be controlled exactly; however, the frequency f can only be approximately controled within a given range by trial and error.

A cyclic triaxial test has four parameters: the average stress ratio $\overline{\eta} = \overline{q}/\mid \overline{p} \mid$, the confinement stress σ_{o}, the cyclic stress amplitude $\sigma_{11}^{\mathrm{cyc}}$ and the excitation frequency f. A low amplitude cyclic excitation corresponds to a small value of the ratio $\zeta^{\mathrm{cyc}} = \sigma_{11}^{\mathrm{cyc}}/\mid \overline{p} \mid$. Table 2 recapitulates the cyclic triaxial tests performed on samples A and B at different static stress states and with different excitation frequencies and amplitudes.

Figure 3 illustrates the time history of the cyclic stress σ_{11} applied on sample B in test

Sample	Test	$\overline{\eta}$	σ_{o} (kPa)	$\sigma_{11}^{\mathrm{cyc}}$ (kPa)	f (Hz)
A	TA1	0.2	50	6	62
	TA2	0.4		3	25
	TA3			6	24
	TA4				67
	TA5				93
	TA6				30
	TA7	0.6			67
B	TB1	0.2	50	6	63
	TB2	0.4			25
	TB3				68
	TB4				100
	TB5	0.6			66

Table 2: Cyclic triaxial tests performed in the current study.

TB2. Under this cyclic excitation, sample B accumulates strain as shown clearly in figure 4. For clarity, this plot is split into three subplots with equal intervals of the axial strain ε_{11}. The strain accumulation is large for the first two cycles and slows down as the cyclic loading continues.

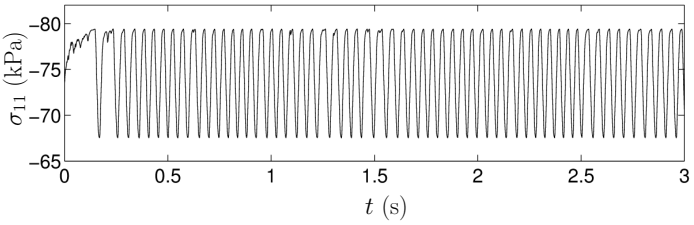

Figure 3: Time history of the cyclic stress σ_{11} applied in test TB2.

In the following, the influence of the sample density, the cyclic excitation amplitude and frequency and the average stress ratio on strain accumulation is analyzed.

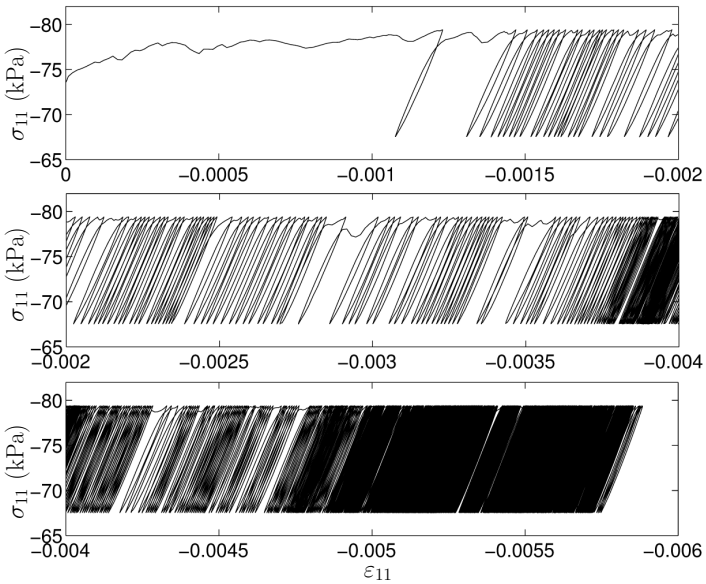

Figure 4: Axial stress σ_{11} versus axial strain ε_{11} in test TB2.

4.1 Influence of the sample density

The influence of the sample density on the intensity and the direction of strain accumulation is analyzed by considering test TA3 performed on sample A and test TB2 performed on sample B. The frequencies of these tests are about 24 Hz. Figure 5 shows the accumulated volumetric strain $\varepsilon_{\mathrm{v}}^{\mathrm{acc}}$ and deviatoric strain $\varepsilon_{\mathrm{d}}^{\mathrm{acc}}$ for samples A and B versus cycle number $\mathcal{N}$. Strain accumulates much more strongly in sample A than in sample B. Both samples accumulate more deviatoric than volumetric strain. In particular, sample A accumulates much more volumetric strain than sample B. This means that loose granular soils are more likely to be compacted during low amplitude cyclic loading than dense soils.

As observed experimentally by many authors [3, 9, 10], the volumetric behavior of a granular sample during cyclic excitation depends on its volumetric behavior at the average stress state. If the sample tends to contract at the average stress state then it contracts during the cyclic excitation. The opposite is observed if the sample tends to dilate at the average stress state. In particular, if the cyclic excitation is applied at the characteristic state then the strain accumulates in the sample with no volume change. These experimental observations can be confirmed by numerical simulation. Indeed, at point A2 in figure 2, sample A contracts strongly; as a result it contracts strongly during test TA3. On the other hand, at point B2 which is near to line $\mathrm{L_B}$, sample B contracts weakly during test TB2.

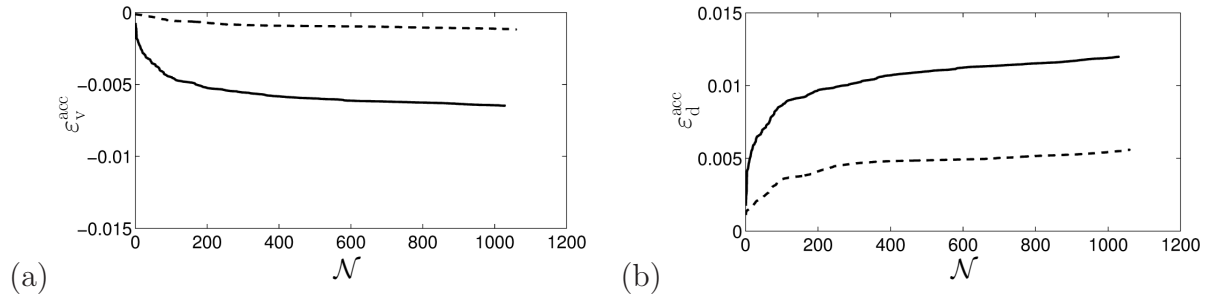

Figure 5: Accumulated (a) volumetric strain $\varepsilon_{\rm v}^{\rm acc}$ and (b) deviatoric strain $\varepsilon_{\rm d}^{\rm acc}$ versus cycle number $\mathcal{N}$ for samples A (solid line) and B (dashed line).

4.2 Effect of the cyclic stress amplitude $\sigma_{11}^{\rm cyc}$

Tests TA2, TA3 and TA6 are performed on sample A at point A2 with different cyclic stress amplitudes $\sigma_{11}^{\rm cyc} = 3$, 6 and 12 kPa. Figure 6 shows that $\sigma_{11}^{\rm cyc}$ influences greatly the strain accumulation in sample A. Both accumulated volumetric and deviatoric strains $\varepsilon_{\rm v}^{\rm acc}$ and $\varepsilon_{\rm d}^{\rm acc}$ increase as $\sigma_{11}^{\rm cyc}$ increases. In addition, at a higher value of $\sigma_{11}^{\rm cyc}$ strain accumulates more rapidly, particularly for about the first 100 cycles. The increase in $\varepsilon_{\rm v}^{\rm acc}$ and $\varepsilon_{\rm d}^{\rm acc}$ with $\sigma_{11}^{\rm cyc}$ can be explained by the fact that a higher excitation amplitude causes more sliding motion between particles to dissipate energy.

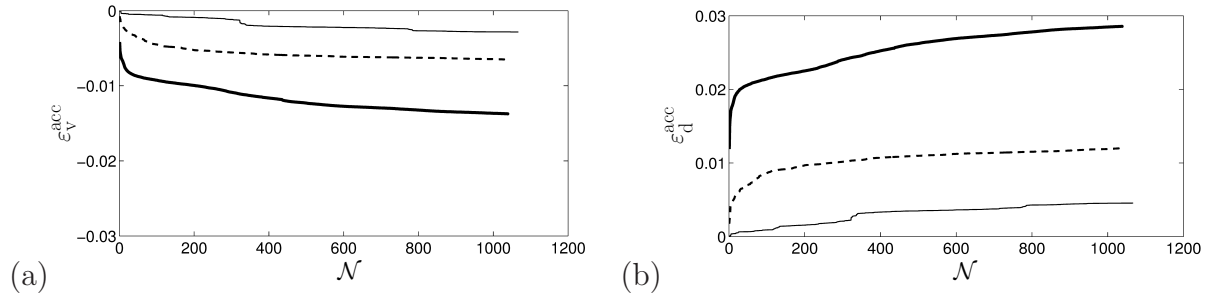

Figure 6: Accumulated (a) volumetric strain $\varepsilon_{\rm v}^{\rm acc}$ and (b) deviatoric strain $\varepsilon_{\rm d}^{\rm acc}$ of sample A versus cycle number $\mathcal{N}$ for a cyclic stress amplitude $\sigma_{11}^{\rm cyc} = 3$ kPa (thin solid line), 6 kPa (dashed line) and 12 kPa (bold solid line).

The density of a granular sample at the microscopic scale is described by the coordination number $\overline{N}$ defined as the average number of contacts per particle

$$\overline{N} = 2\frac{N_{\rm c}}{N_{\rm p}}, \tag{1}$$

with $N_{\rm c}$ the number of contacts and $N_{\rm p}$ the number of particles. Kuhn [11] introduced the effective coordination number $\overline{N}_{\rm eff}$ by removing all the floating particles (particles that

have no more than 3 contacts with their neighbors) from the sample when calculating the coordination number $\overline{N}$. Figure 7 shows the evolution of the effective coordination number $\overline{N}_{\text{eff}}$ of sample A during cyclic loading for different values of the cyclic stress amplitute σ_{11}^{cyc}. A marked increase of $\overline{N}_{\text{eff}}$ is observed for $\sigma_{11}^{\text{cyc}} = 12$ kPa, while $\overline{N}_{\text{eff}}$ remains almost constant for $\sigma_{11}^{\text{cyc}} = 3$ kPa. The dependence of $\overline{N}_{\text{eff}}$ on σ_{11}^{cyc} results from the fact that the sample densifies more strongly at a higher value of σ_{11}^{cyc} (figure 6).

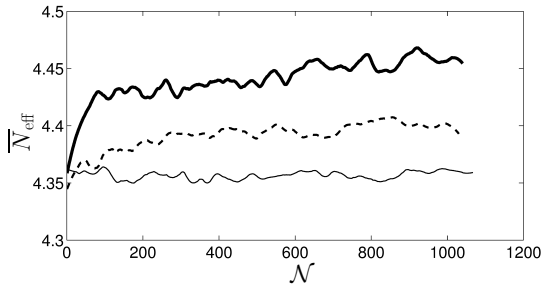

Figure 7: Effective coordination number $\overline{N}_{\text{eff}}$ of sample A versus cycle number $\mathcal{N}$ for a cyclic stress amplitude $\sigma_{11}^{\text{cyc}} = 3$ kPa (thin solid line), 6 kPa (dashed line) and 12 kPa (bold solid line).

4.3 Influence of the cyclic excitation frequency f

Tests TA3, TA4 and TA5 are performed on sample A at different excitation frequencies $f = 24$, 67 and 93 Hz and tests TB2, TB3 and TB4 are performed on sample B at $f = 25$, 68 and 100 Hz. The magnitude ε^{acc} of the accumulated strain is defined as Frobenius norm of the accumulated strain tensor $\boldsymbol{\varepsilon}^{\text{acc}}$. For triaxial loading, $\boldsymbol{\varepsilon}^{\text{acc}}$ is diagonal; therefore, $\varepsilon^{\text{acc}} = \|\boldsymbol{\varepsilon}^{\text{acc}}\|_{\text{F}} = \sqrt{(\varepsilon_{11}^{\text{acc}})^2 + (\varepsilon_{22}^{\text{acc}})^2 + (\varepsilon_{33}^{\text{acc}})^2}$.

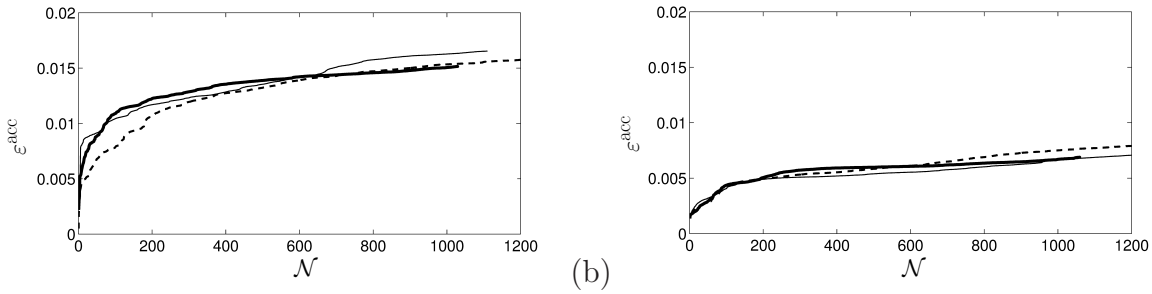

Figure 8: Accumulated strain ε^{acc} versus cycle number $\mathcal{N}$ (a) for sample A at a cyclic excitation frequency 24 Hz (bold solid line), 67 Hz (dashed line) and 93 Hz (thin solid line) and (b) for sample B at 25 Hz (bold solid line), 68 Hz (dashed line) and 100 Hz (thin solid line).

The magnitude ε^{acc} of the accumulated strain is plotted versus the cycle number $\mathcal{N}$ for samples A and B in figure 8. The cyclic excitation frequency f has little effect on strain

accumulation in these samples. For sample A, ε^{acc} is about 0.015 at 24 Hz after 1000 cycles, compared to a value of 0.016 at 93 Hz. This result might be explained by the fact that, for the considered values of the excitation frequency, samples A and B are still in the quasi-static regime.

4.4 Effect of the average stress ratio $\overline{\eta}$

Tests TA1, TA4 and TA7 on sample A at points A1, A2 and A3 and tests TB1, TB3 and TB5 on sample B at points B1, B2 and B3 are considered to analyze the effect of the average stress ratio $\overline{\eta}$ on strain accumulation. Note that $\overline{\eta} = 0.2$ at points A1 and B1, $\overline{\eta} = 0.4$ at points A2 and B2 and $\overline{\eta} = 0.6$ at points A3 and B3 (figure 2). These tests are performed at a high frequency of approximately 65 Hz. The number of cycles is about 8000 for the tests performed on sample A and 2000 for the tests performed on sample B.

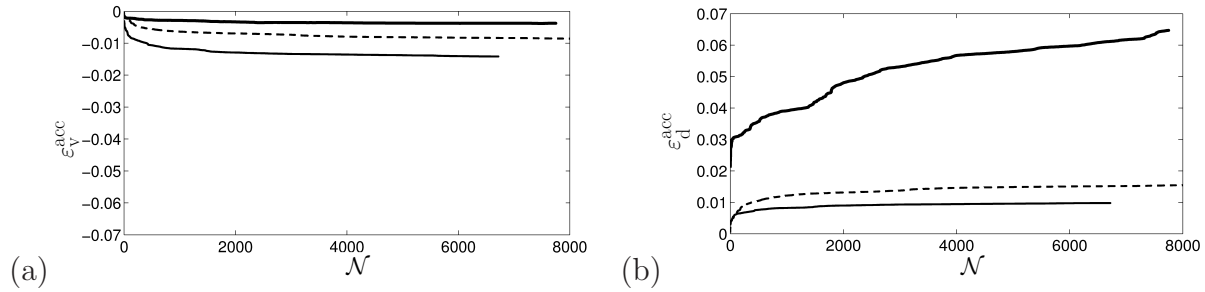

Figure 9: Accumulated (a) volumetric strain $\varepsilon_{\text{v}}^{\text{acc}}$ and (b) deviatoric strain $\varepsilon_{\text{d}}^{\text{acc}}$ versus cycle number $\mathcal{N}$ for sample A at an average stress ratio $\overline{\eta} = 0.2$ (thin solid line), 0.4 (dashed line) and 0.6 (bold solid line).

The accumulated strain in sample A depends strongly on the average stress ratio $\overline{\eta}$, particularly for the accumulated deviatoric strain $\varepsilon_{\text{d}}^{\text{acc}}$, as indicated in figure 9. Strain accumulates much more strongly in sample A for $\overline{\eta} = 0.6$ than for $\overline{\eta} = 0.2$ and 0.4, in particular for the first 10 cycles. After 6000 cycles, $\varepsilon_{\text{d}}^{\text{acc}}$ reaches a large value of 0.06 for $\overline{\eta} = 0.6$, compared to a value of 0.015 for $\overline{\eta} = 0.4$ and 0.01 for $\overline{\eta} = 0.2$. In addition, for $\overline{\eta} = 0.6$ strain still accumulates substantially in sample A after 7000 cycles, while for $\overline{\eta} = 0.2$ and 0.4, strain accumulation almost ceases after 1000 cycles. A similar effect of the average stress ratio $\overline{\eta}$ on strain accumulation is observed on sample B (figure 10). The accumulated volumetric strain $\varepsilon_{\text{v}}^{\text{acc}}$ is negligible compared to the deviatoric strain $\varepsilon_{\text{d}}^{\text{acc}}$. The accumulated strain is almost zero during the cyclic excitation applied at $\overline{\eta} = 0.2$ as the behavior of sample B is highly elastic at this average stress state (figure 2).

The fabric of a granular sample is described by the following tensor:

$$H_{ij} = \frac{1}{N_{\text{c}}} \sum_{k=1}^{N_{\text{c}}} n_i^k n_j^k, \tag{2}$$

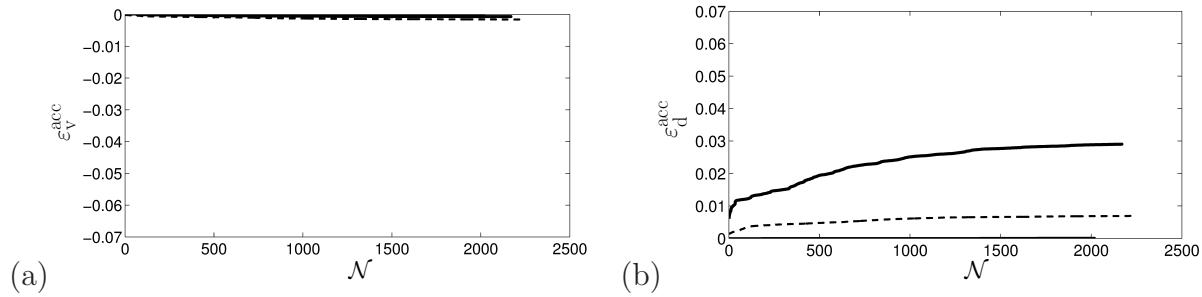

Figure 10: Accumulated (a) volumetric strain $\varepsilon_{\rm v}^{\rm acc}$ and (b) deviatoric strain $\varepsilon_{\rm d}^{\rm acc}$ versus cycle number $\mathcal{N}$ for sample B at an average stress ratio $\overline{\eta} = 0.2$ (thin solid line), 0.4 (dashed line) and 0.6 (bold solid line).

where n_i^k is the i-th component of the unitary normal vector at contact k [12]. For triaxial loading, H_{11}, H_{22} and H_{33} are the three principal values and $H_{22} \approx H_{33}$. In this case, the anisotropy of a sample can be measured by $H_{\rm d} = H_{11} - H_{33}$. The effect of the average stress ratio $\overline{\eta}$ on the evolution of the anisotropy of sample A is shown in figure 11. The average stress ratio $\overline{\eta}$ affects greatly the anisotropy induced by the consolidation phase, but not the anisotropy induced by low amplitude cyclic excitation. The anisotropy of the sample remains almost constant during the applied cylic excitations whatever the value of $\overline{\eta}$ is.

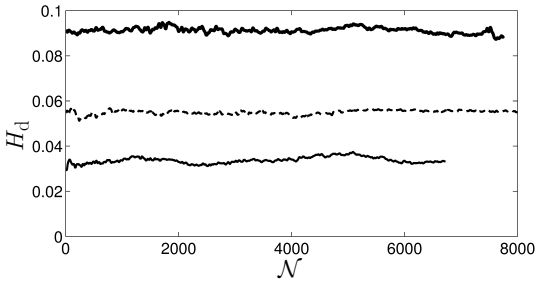

Figure 11: Anisotropy measure $H_{\rm d}$ versus cycle number $\mathcal{N}$ for sample A at an average stress ratio $\overline{\eta} = 0.2$ (thin solid line), 0.4 (dashed line) and 0.6 (bold solid line).

5 CONCLUSIONS

A series of simulations with the DEM was carried out to study strain accumulation in granular materials subjected to low amplitude cyclic loading. A loose and a medium dense sample composed of about 10000 spheres were considered in these simulations. The study has shown that the loose sample accumulates much more strain than the dense one during cyclic excitation. The strain accumulation increases with the cyclic stress amplitude and the average stress ratio; however, it is not affected by the cyclic excitation frequency

up to 100 Hz. At the microscopic scale, the internal structure of the samples evolves slightly during cyclic loading. An increase in the coordination number observed for the loose sample is due to its densification during cyclic excitation. However, the anisotropy of these samples induced by low amplitude cyclic excitation is negligible compared to the anisotropy induced by the consolidation phase. The DEM is able to reproduce, at least in a qualitative sense, the strain accumulation phenomenon observed in laboratory experiments. To advance the use of the DEM to study this topic, more realistic particle shapes should be accounted for in simulations.

References

[1] G. Lombaert and G. Degrande. The experimental validation of a numerical model for the prediction of the vibrations in the free field produced by road traffic. *Journal of Sound and Vibration*, 262:309–331, 2003.

[2] G. Lombaert, G. Degrande, J. Kogut, and S. François. The experimental validation of a numerical model for the prediction of railway induced vibrations. *Journal of Sound and Vibration*, 297:512–535, 2006.

[3] T. Wichtmann, A. Niemunis, and Th. Triantafyllidis. Strain accumulation in sand due to cyclic loading: drained triaxial tests. *Soil Dynamics and Earthquake Engineering*, 25:967–979, 2005.

[4] T. Wichtmann. *Explicit accumulation model for non-cohesive soils under cyclic loading*. PhD thesis, Des Institutes Für Grundbau Und Bodenmechanik Der Ruhr-Universität-Bochum, Bochum, Germany, 2005.

[5] C. Karg. *Modelling of strain accumulation due to low level vibrations in granular soils*. PhD thesis, Ghent University, Ghent, Belgium, 2007.

[6] P.A. Cundall and O.D.L. Strack. A discrete numerical model for granular assemblies. *Géotechnique*, 29(1):47–65, 1979.

[7] Itasca Consulting Group Inc. *PFC3D: Theory and Background*, 2008.

[8] C. O'Sullivan. *Particulate Discrete Element Modelling: A Geomechanics Perspective*. Applied Geotechnics Volume 4. Spon Press, 2011.

[9] M.P. Luong. Mechanical aspects and thermal effects of cohesionless soils under cyclic and transient loading. In *IUTAM Conference on Deformation and Failure of Granular Materials*, pages 239–246, Delft, 1982.

[10] C.S. Chang and R.V. Whitman. Drained permanent deformation of sand due to cyclic loading. *Journal of Geotechnical Engineering*, 114:1164–1180, 1988.

[11] M.R. Kuhn. Structured deformation in granular materials. *Mechanics of Materials*, 31:407–429, 1999.

[12] M. Satake. Fabric tensor in granular materials. In P. Vermeer and H. Luger, editors, *IUTAM Symposium on Deformation and Failure of Granular Materials*, pages 63–68. A.A. Balkema, 1982.